

Supplementary Materials for  
**Calcium channel  $\beta$ 3 subunit regulates ATP-dependent migration of  
dendritic cells**

Marcel S. Woo *et al.*

Corresponding author: Manuel A. Friese, [manuel.friese@zmnh.uni-hamburg.de](mailto:manuel.friese@zmnh.uni-hamburg.de)

*Sci. Adv.* **9**, eadh1653 (2023)  
DOI: 10.1126/sciadv.adh1653

**This PDF file includes:**

Figs. S1 to S8  
Table S1

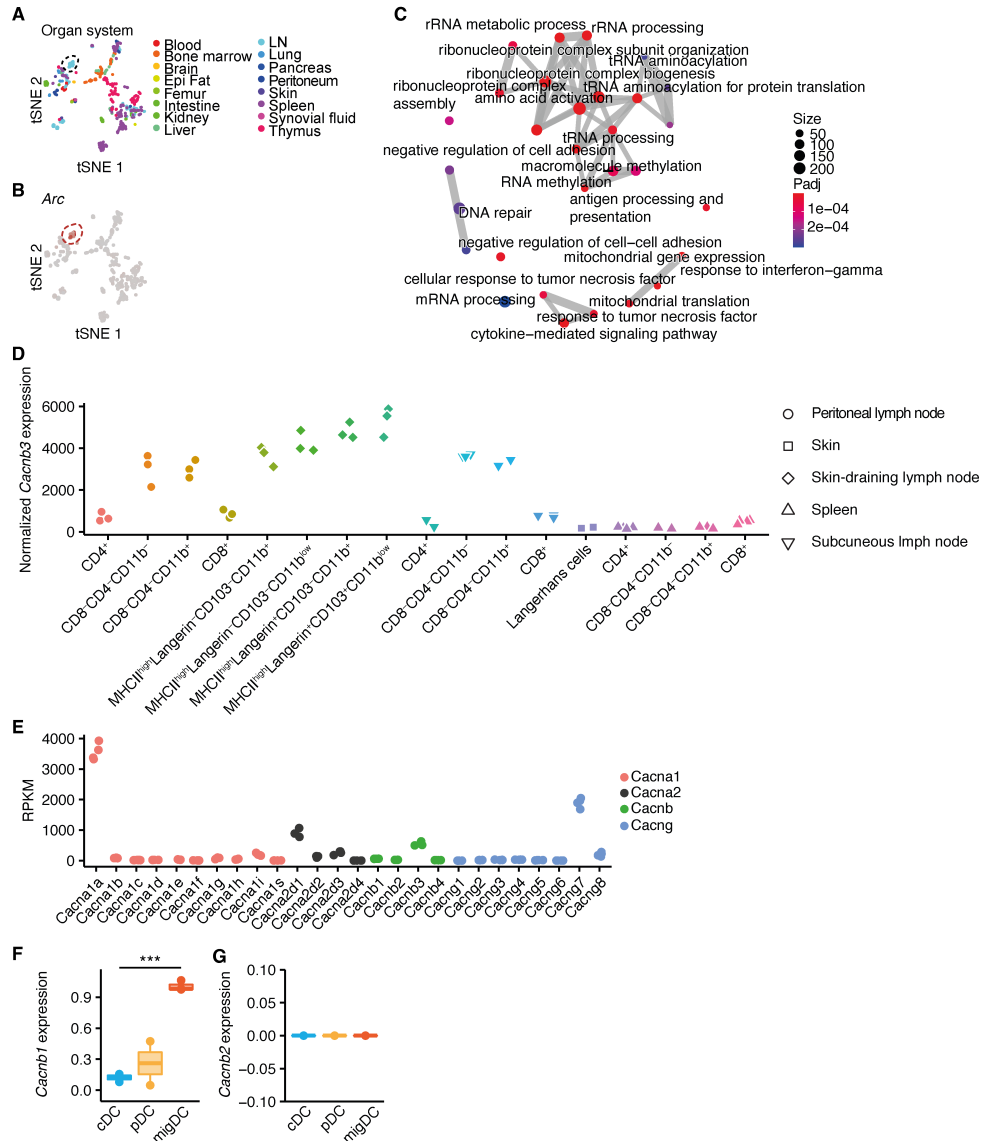


**Fig. S1. migDCs are defined by CACNB3 expression.** (A) tSNE representation of all included 653 samples from the ImmGen database (GSE15907) (25–27). Color indicates the annotated organ system from which the samples were originally retrieved. (B) tSNE representation of all included 653 samples from the ImmGen database (GSE15907). migDCs are highlighted, color shows *Arc* expression. (C) GO term biological process enrichment analysis of migDC-defining genes. Color shows adjusted *P*-values, size shows number of genes. (D) Normalized expression of *Cacnb3* in indicated DC subsets in lymph nodes, spleen and skin retrieved from the ImmGen database (GSE15907), color indicates different subsets, shape represents organs where cells were sorted from. (E) Reads per kilobase of transcript per million mapped reads (RPKM) of voltage-gated calcium channel subunits from primary neuronal cultures in RNA-sequencing ( $n = 3$ ). (F and G) Relative expression of *Cacnb1* (F) and *Cacnb2* (G) in sorted cDCs, pDCs, and migDCs. If not stated otherwise unpaired *t*-test was used for statistical comparison, \*\*\* $P < 0.001$ .

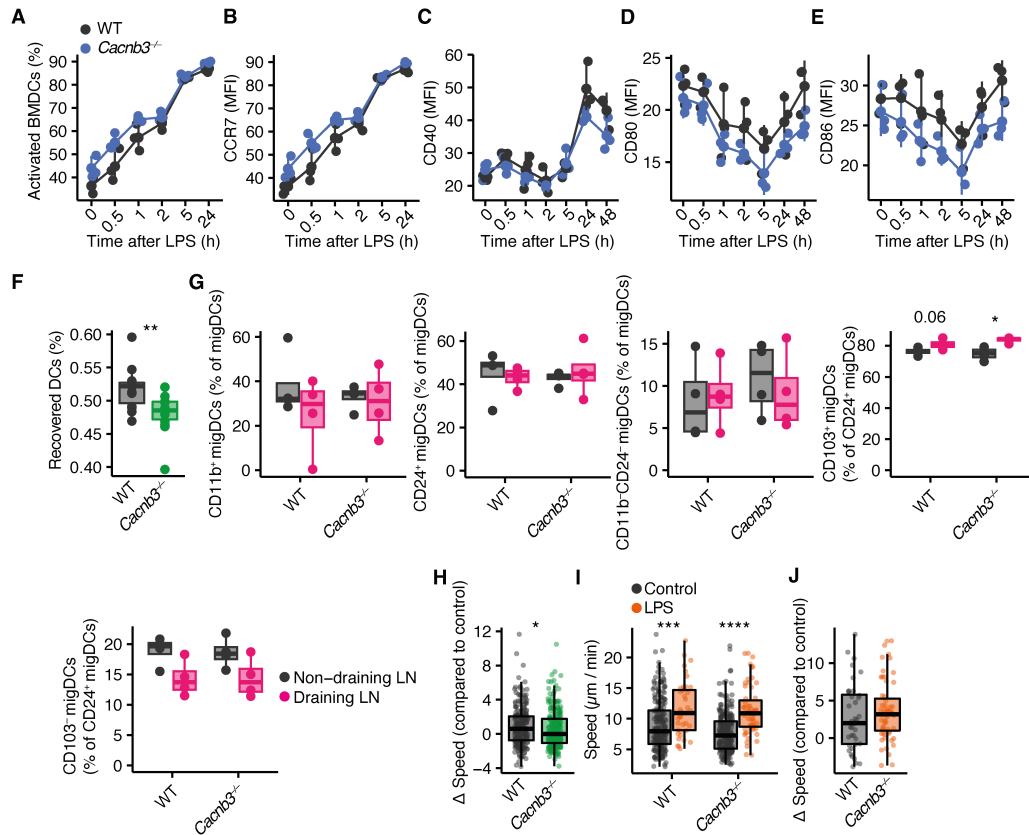


**Fig. S2. LPS-induced activation and migration of BMDCs is independent of CACNB3.** (A to E) Percentage of MHCII high BMDCs (A), CCR7 MFI (B), CD40 MFI (C), CD80 MFI (D) and CD86 MFI (E) of BMDCs from WT and *Cacnb3*<sup>-/-</sup> animals ( $n = 3$ ) at different time points after stimulation with  $100 \text{ ng mL}^{-1}$  LPS. (F) Relative frequency of recovered migDCs in ipsilateral cervical lymph nodes after ear tape stripping experiment #2 ( $n = 9$ ). (G) Percentage of different migDC subsets in draining and non-draining cervical lymph nodes after ear tape-stripping in WT and *Cacnb3*<sup>-/-</sup> animals ( $n = 4$ ). (H) Speed difference of ATP-stimulated BMDCs from WT and *Cacnb3*<sup>-/-</sup> animals in comparison to vehicle-stimulated controls. (I) Quantification of mean speed ( $\mu\text{m min}^{-1}$ ) of WT and *Cacnb3*<sup>-/-</sup> BMDCs that were imaged in microchannels after pulsing with vehicle or  $100 \text{ ng mL}^{-1}$  LPS. (J) Speed difference of LPS-stimulated BMDCs from WT and *Cacnb3*<sup>-/-</sup> animals in comparison to vehicle stimulated controls. If not stated otherwise unpaired  $t$ -test was used for statistical comparison, \* $P < 0.05$ , \*\* $P < 0.01$ , \*\*\* $P < 0.001$ , \*\*\*\* $P < 0.0001$ .

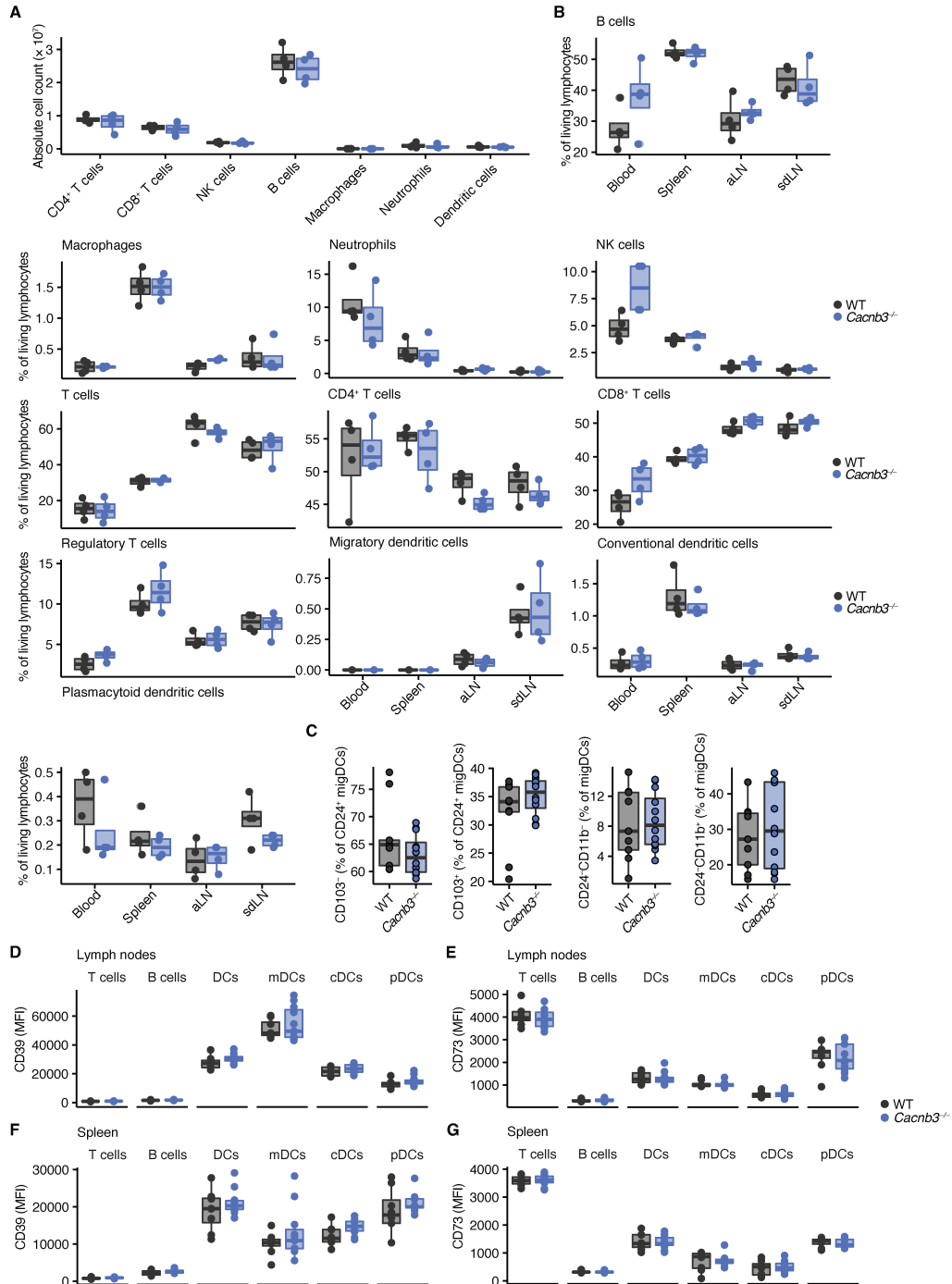


**Fig. S3. Immune cell composition is not changed in *Cacnb3*-deficient animals in steady-state.** (A) Absolute numbers of immune cell subsets in the spleens of healthy WT and *Cacnb3*<sup>-/-</sup> mice ( $n = 4$ ). (B) Relative frequencies of immune cell subsets in blood, spleen, aortic lymph nodes (aLN), skin-draining lymph nodes (sdLN) of WT and *Cacnb3*<sup>-/-</sup> mice ( $n = 4$ ). (C) Relative percentage of shown migDC subsets isolated from sdLNs of healthy WT ( $n = 9$ ) and *Cacnb3*<sup>-/-</sup> mice ( $n = 12$ ). (D and E) CD39 MFI (D) and CD73 MFI (E) in sLN nodes of WT ( $n = 6$ ) and *Cacnb3*<sup>-/-</sup> ( $n = 8$ ) mice of respective immune cell subsets. (F and G) CD39 MFI (F) and CD73 MFI (G) in spleens of WT ( $n = 6$ ) and *Cacnb3*<sup>-/-</sup> ( $n = 8$ ) of shown immune cell subsets. If not stated otherwise unpaired *t*-test was used for statistical comparison.

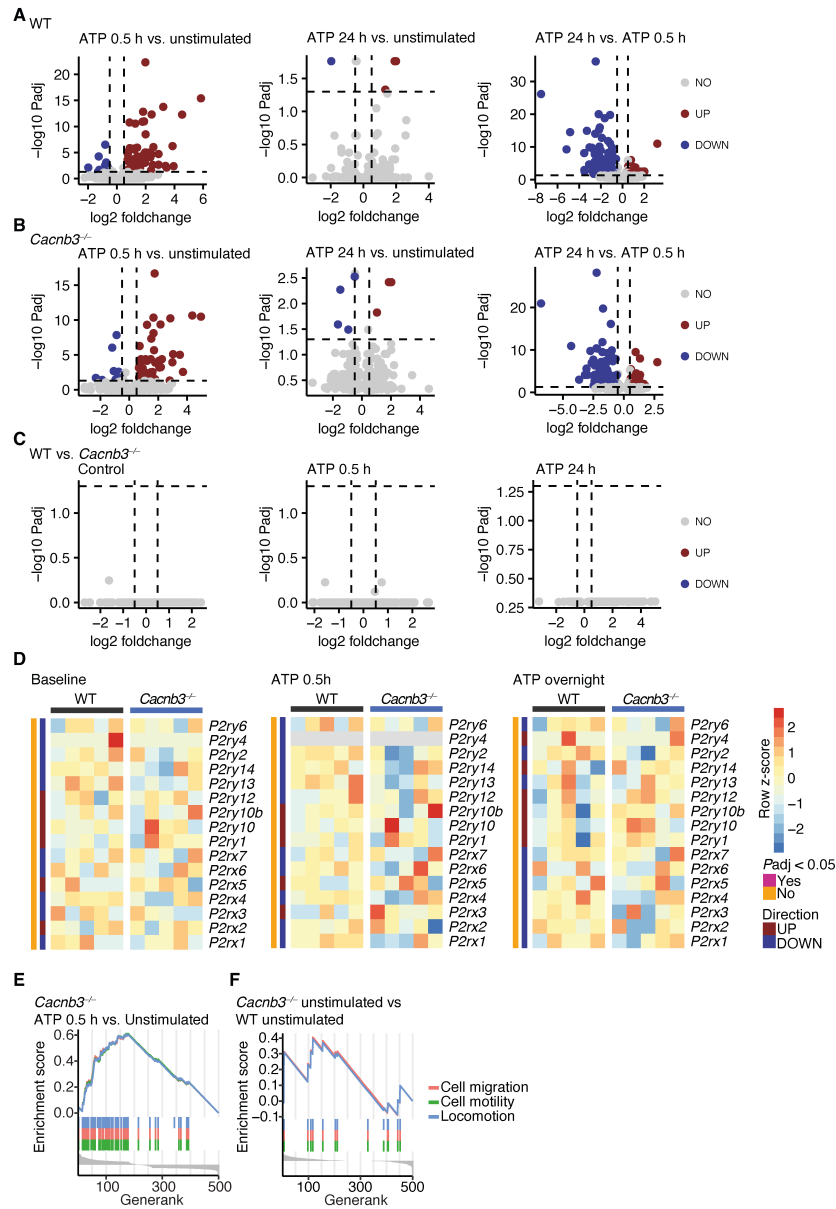


**Fig. S4. No differential gene expression between WT and *Cacnb3*-deficient BMDCs.** (A to C) Volcano plots depicting RNA sequencing results of WT (A) and *Cacnb3*<sup>-/-</sup> (B) BMDCs after 30 min pulse with 500  $\mu$ M ATP and 24 h after ATP pulse and comparisons between genotypes (C). The comparisons are detailed in the figure. Differentially up- or downregulated genes with *P*<sub>adj</sub> < 0.05 and log<sub>2</sub> foldchange > 0.5 or < -0.5 are colored in the plots. (D) Expression of all identified P2XR and P2YR in our RNA-sequencing datasets. Comparisons between WT and *Cacnb3*<sup>-/-</sup> BMDCs at baseline (left), directly after (middle) or after overnight incubation (right) following 30 min pulse with 500  $\mu$ M ATP are shown. Color shows row z-score. No significant differences were found. (E) GO term enrichment analyses of GO terms “Cell migration” (NES = 1.58, *P*<sub>adj</sub> = 0.002), “Cell motility” (NES = 1.57, *P*<sub>adj</sub> = 0.002) and “Locomotion” (NES = 1.58, *P*<sub>adj</sub> = 0.001) in *Cacnb3*<sup>-/-</sup> BMDCs after 30 min ATP pulse in our RNA-sequencing experiment. All GO terms *P*-value < 0.01. (F) GO term enrichment analyses of GO terms “Cell migration” (NES = -1.4, *P*<sub>adj</sub> = 0.42), “Cell motility” (NES = -1.33, *P*<sub>adj</sub> = 0.46) and “Locomotion” (NES = -1.23, *P*<sub>adj</sub> = 0.52) in differentially expressed genes between WT and *Cacnb3*<sup>-/-</sup> BMDCs in our RNA-sequencing experiment. All GO terms *P*-value > 0.05.

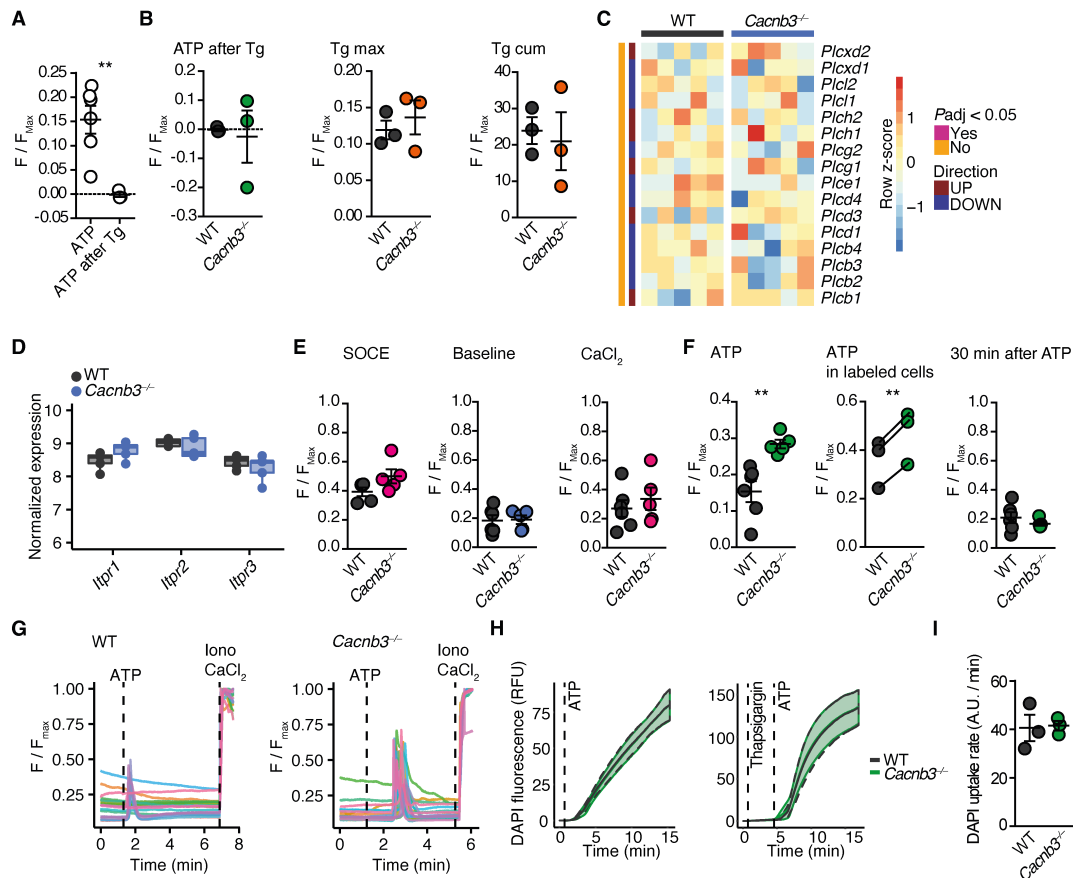


**Fig. S5. Cacnb3 deficiency does not change ATP-induced DAPI uptake.** (A) Maximal calcium response after 500  $\mu$ M ATP stimulation alone or 500  $\mu$ M ATP stimulation after 1  $\mu$ M thapsigargin (Tg) application. (B) Comparison of maximal calcium response of WT and *Cacnb3*<sup>-/-</sup> BMDCs after 500  $\mu$ M ATP stimulation after application of 1  $\mu$ M thapsigargin (Tg; left). Maximal (middle) and cumulative (right) calcium response after stimulation with 1  $\mu$ M thapsigargin (Tg) of WT and *Cacnb3*<sup>-/-</sup> BMDCs. (C) Gene expression of PLC subunits in steady-state WT and *Cacnb3*<sup>-/-</sup> BMDCs from our RNA-sequencing data. None of the depicted genes were differentially expressed. Color shows row z-score. (D) Normalized expression from our RNA-sequencing experiment of *Itpr1*, *Itpr2* and *Itpr3* in WT and *Cacnb3*<sup>-/-</sup> BMDCs ( $n = 5$ ). (E) Maximal calcium response after store-operated calcium entry (SOCE) activation of Fluo-4 loaded WT and *Cacnb3*<sup>-/-</sup> BMDCs by subsequent depletion of calcium with 2 mM EGTA and 1  $\mu$ M thapsigargin for 10 minutes and subsequent application of 2 mM calcium chloride (left), at baseline (middle) or application of calcium 2 mM CaCl<sub>2</sub> (right). (F) Maximal calcium responses of Fluo-4 loaded WT and *Cacnb3*<sup>-/-</sup> BMDCs that were stimulated with 500  $\mu$ M ATP (left;  $n = 5$ ), and of *Cacnb3*<sup>-/-</sup> BMDCs that were fluorescently labeled and mixed in a 1:1 ratio and were stimulated with 500  $\mu$ M ATP (middle;  $n = 3$ ), and calcium signal 30 minutes after stimulation with 500  $\mu$ M ATP (right;  $n = 5$ ). Paired  $t$ -test was used for comparison of calcium levels in labeled cells. (G) Representative calcium traces of 20 randomly selected cells from WT (left) and *Cacnb3*<sup>-/-</sup> (right) BMDCs that were loaded with Fluo-4 and were exposed to 500  $\mu$ M ATP,  $F/F_{max}$  are shown. (H) Pooled traces of DAPI fluorescence of living WT and *Cacnb3*<sup>-/-</sup> BMDCs after stimulation with 500  $\mu$ M ATP alone or after application of 1  $\mu$ M thapsigargin. (I) Quantification of area under the curve per minute of DAPI uptake after ATP stimulation of living WT and *Cacnb3*<sup>-/-</sup> BMDCs ( $n = 3$ ). If not stated otherwise unpaired  $t$ -test was used for statistical comparison, \*\* $P < 0.01$ .

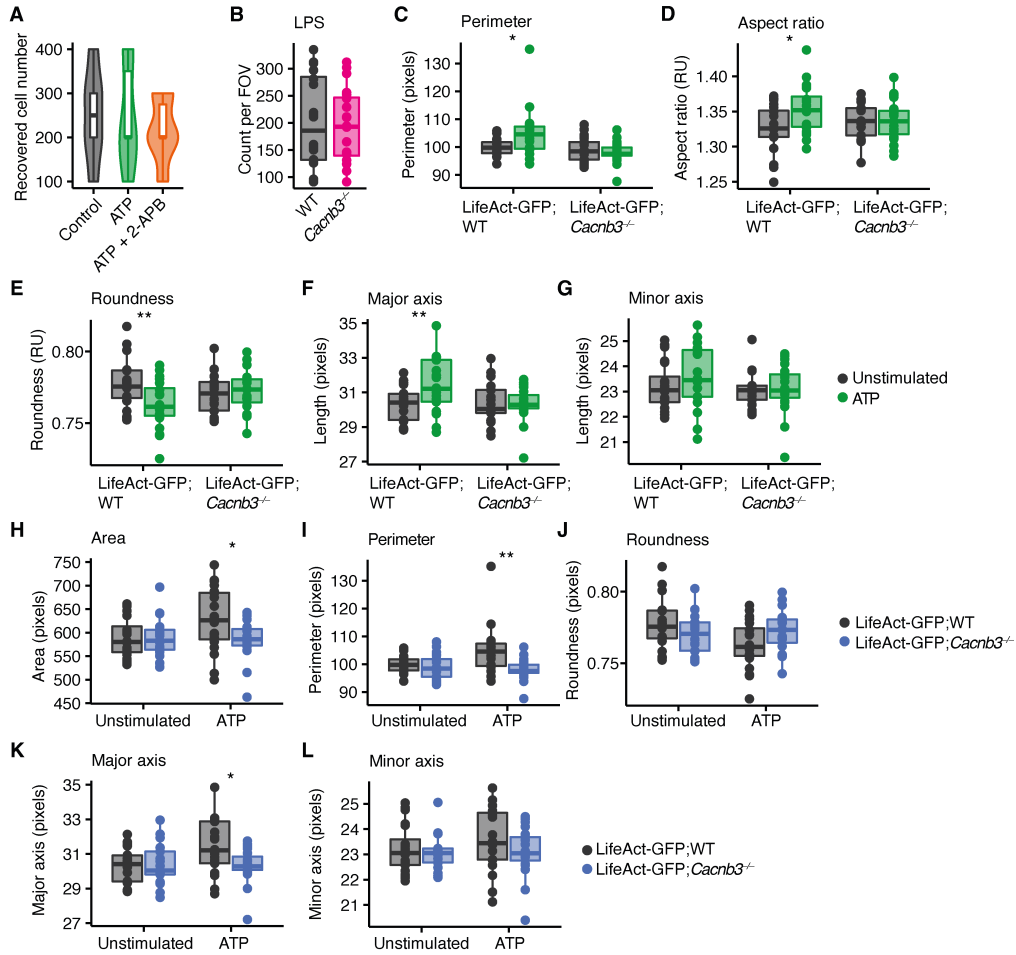


**Fig. S6. Morphometric changes of WT and *Cacnb3*-deficient BMDCs after ATP stimulation.** (A) Recovered cell number in Boyden chamber 2 h after stimulation with vehicle, 500  $\mu$ M ATP 30 min pulse, 500  $\mu$ M ATP pulse with 50  $\mu$ M 2-APB and 1  $\mu$ M thapsigargin ( $n = 6$ ). (B) Count per FOV 6 h after 30 min pulse with 100 ng mL<sup>-1</sup> LPS of WT and *Cacnb3*<sup>-/-</sup> BMDCs ( $n = 20$ ). (C to G) Comparison of perimeter (C), aspect ratio (D), roundness (E), major axis (F), minor axis (G) after vehicle and 6 h after a 30 min pulse with 500  $\mu$ M ATP of BMDCs from *LifeAct-GFP*;WT and *LifeAct-GFP*;*Cacnb3*<sup>-/-</sup> mice ( $n = 20$ ). Comparisons between unstimulated and ATP stimulated BMDCs within respective genotypes are shown. (H to L) Comparison of perimeter (H), aspect ratio (I), roundness (J), major axis (K), minor axis (L) of BMDCs from *LifeAct-GFP*;WT and *LifeAct-GFP*;*Cacnb3*<sup>-/-</sup> mice after vehicle and 6 h after 30 min pulse stimulation with 500  $\mu$ M ATP ( $n = 20$ ). Comparisons between genotypes in vehicle- or ATP-stimulated BMDCs are shown. If not stated otherwise unpaired *t*-test was used for statistical comparison, \* $P < 0.05$ , \*\* $P < 0.01$ , \*\*\* $P < 0.001$ , \*\*\*\* $P < 0.0001$ .

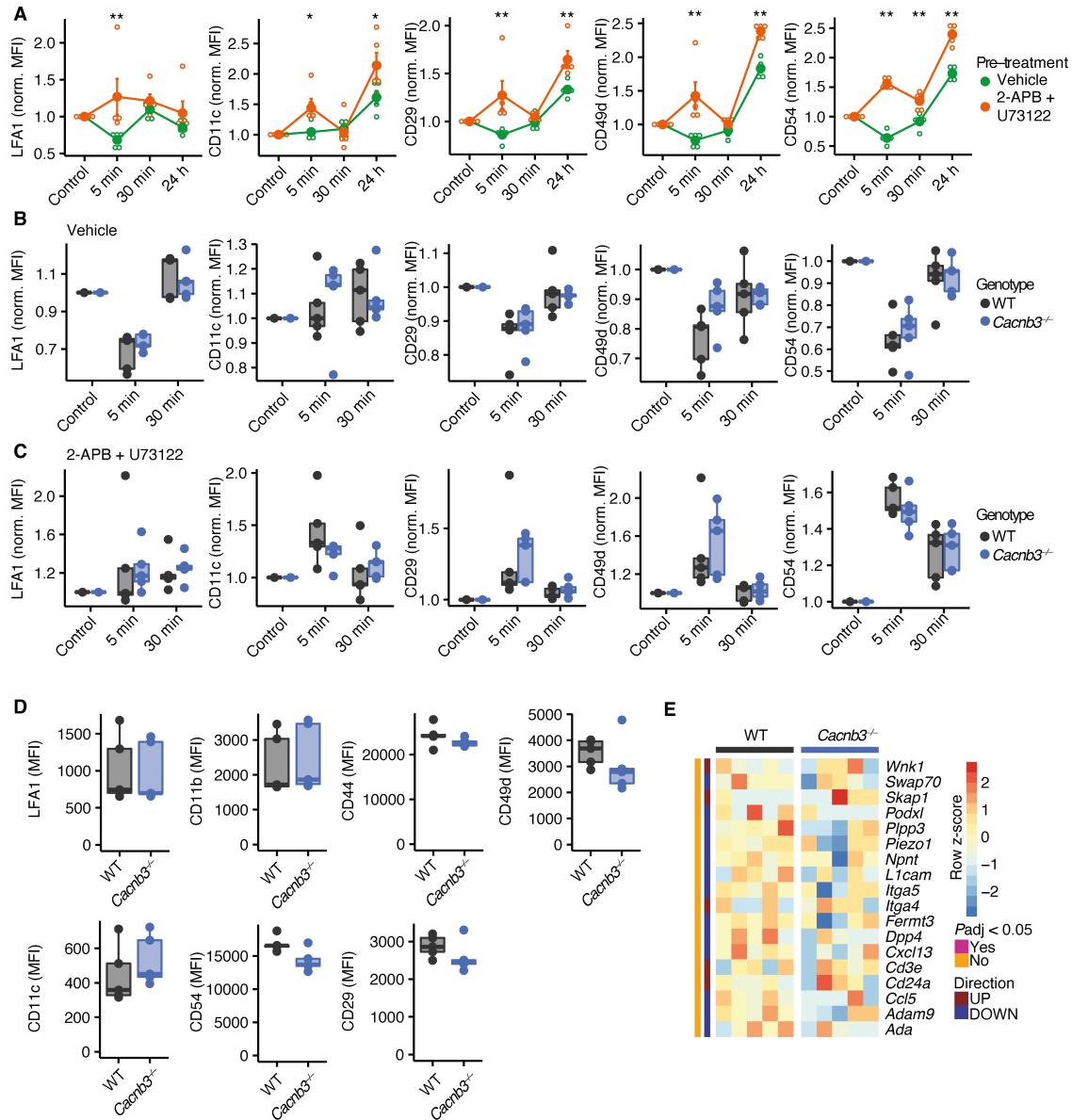


**Fig. S7. Dynamic changes of adhesion molecule surface expression after ATP stimulation. (A)** MFI of LFA1, CD11c, CD29, CD49d, CD54 after vehicle stimulation or 5 min, 30 min or 24 h after stimulation with 500  $\mu$ M ATP or 500  $\mu$ M ATP together with 50  $\mu$ M 2-APB and 1  $\mu$ M U73122 ( $n = 5$ ). **(B)** Normalized MFI of LFA1, CD11c, CD29, CD49d, CD54 after vehicle stimulation or 5 min, 30 min or 24 h after stimulation with 500  $\mu$ M ATP in WT and *Cacnb3*<sup>-/-</sup> BMDCs ( $n = 5$ ). Data were normalized to controls of each genotype. **(C)** Normalized MFI of LFA1, CD11c, CD29, CD49d, CD54 after vehicle stimulation or 5 min, 30 min or 24 h after stimulation with 500  $\mu$ M ATP with 50  $\mu$ M 2-APB and 1  $\mu$ M U73122 in WT and *Cacnb3*<sup>-/-</sup> BMDCs ( $n = 5$ ). Data were normalized to controls of each genotype. **(D)** Raw MFI of LFA1, CD11b, CD44, CD49d, CD11c, CD54 and CD29 in WT and *Cacnb3*<sup>-/-</sup> BMDCs ( $n = 5$ ) at steady-state. **(E)** Expression of depicted adhesion molecules in RNA-sequencing dataset of WT and *Cacnb3*<sup>-/-</sup> BMDCs at steady-state. Color shows row z-score. If not stated otherwise unpaired *t*-test was used for statistical comparison, \* $P < 0.05$ , \*\* $P < 0.01$ .

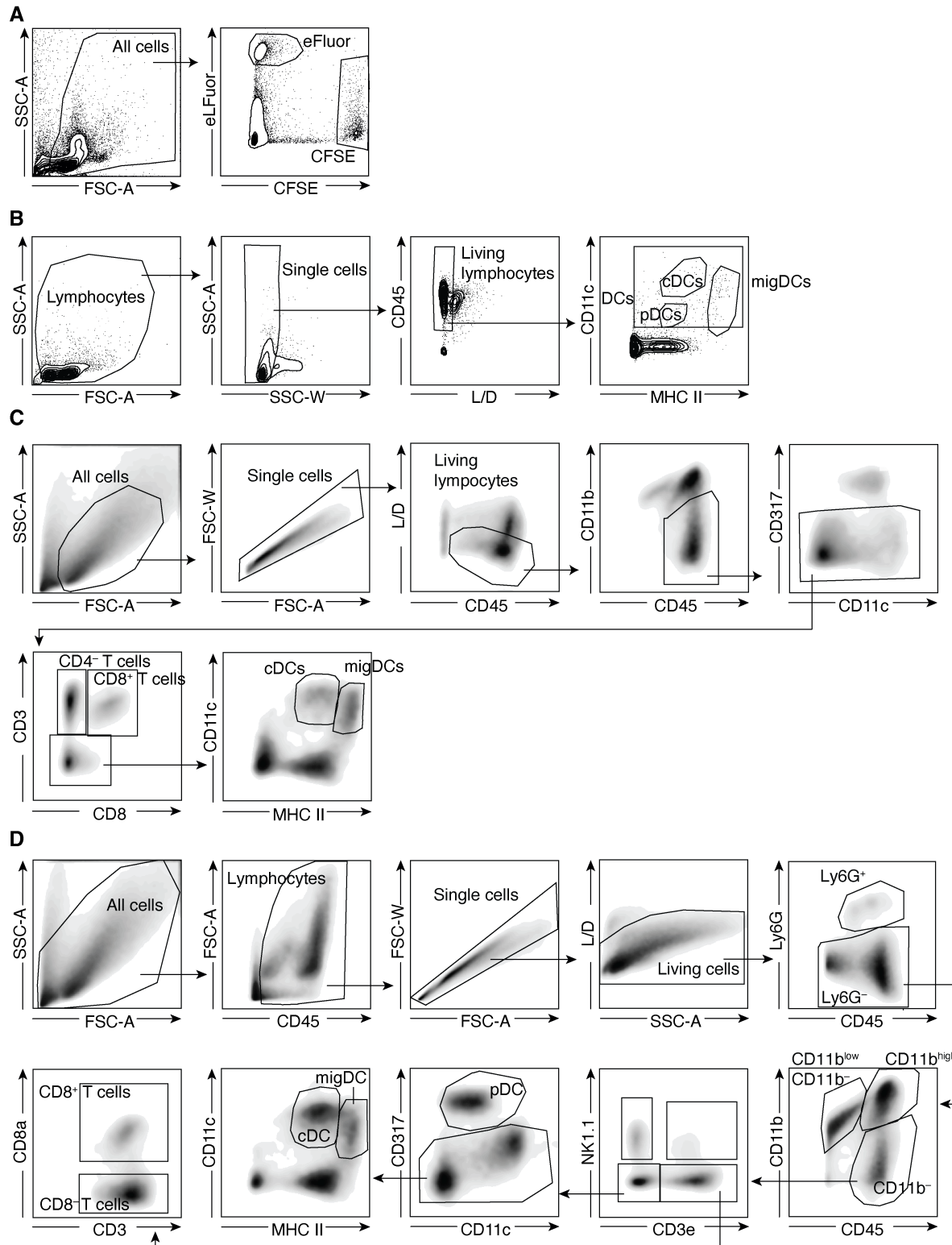


**Fig. S8. Representative gating strategies.** (A) Identification of labeled BMDCs after footpad injection. (B) Sorting strategy for different DC populations. (C) Identification of DCs by flow cytometry. (D) Peripheral immune cell phenotyping.

**Table S1. List of antibodies used in this study.**

<b>Antigen</b>	<b>Host species</b>	<b>Company</b>	<b>Catalogue no.</b>	<b>Ig fraction</b>	<b>Fluorophore</b>	<b>Dilution FACS</b>
<b>CACNB3</b>	Rabbit	generated in-house		IgG		
<b>CD3ε</b>	Armenian hamster	BioLegend	100305	IgG	FITC	1:100
<b>CD8a</b>	Rat	BioLegend	100750	IgG	BV785	1:200
<b>CD11b</b>	Rat	BD Biosciences	563553	IgG	BUV395	1:200
<b>CD11b</b>	Rat	BioLegend	101228	IgG	PerCP-Cy5.5	1:400
<b>CD11c</b>	Armenian hamster	BioLegend	117336	IgG	BV786	1:300
<b>CD11c</b>	Armenian hamster	BioLegend	117318	IgG	PE-Cy7	1:300
<b>CD19</b>	Rat	BioLegend	115541	IgG	BV650	1:400
<b>CD19</b>	Rat	BioLegend	115506	IgG	FITC	1:100
<b>CD29</b>	Armenian Hamster	BioLegend	102205	IgG	FITC	1:200
<b>CD39</b>	Rat	BioLegend	143808	IgG	AF647	1:300
<b>CD40</b>	Rat	BioLegend	124612	IgG	APC	1:100
<b>CD44</b>	Rat	BioLegend	103049	IgG	BV650	1:200
<b>CD45</b>	Rat	BioLegend	103127	IgG	AF700	1:200
<b>CD45</b>	Rat	BioLegend	103112	IgG	APC	1:200
<b>CD49d</b>	Rat	BioLegend	103608	IgG	PE	1:100
<b>CD54 (ICAM-1)</b>	Rat	BioLegend	116121	IgG	PE-Cy7	1:400
<b>CD73</b>	Rat	BioLegend	127206	IgG	PE	1:200
<b>CD80</b>	Armenian hamster	BioLegend	104705	IgG	FITC	1:100
<b>CD86</b>	Rat	BD Biosciences	750437	IgG	BUV496	1:200
<b>CD197</b>	Rat	BioLegend	120105	IgG	PE	1:100
<b>CD205</b>	Rat	BioLegend	138213	IgG	PE	1:200
<b>CD272 (BTLA)</b>	Rat	BioLegend	134809	IgG	PE-Cy7	1:100
<b>CD274 (PD-L1)</b>	Rat	BioLegend	124311	IgG	BV650	1:100
<b>CD279 (PD-1)</b>	Rat	BioLegend	135224	IgG	APC	1:100
<b>CD317 (PDCA1)</b>	Rat	BioLegend	127016	IgG	APC	1:100
<b>CD317 (PDCA1)</b>	Rat	BioLegend	127103	IgG	PE	1:100
<b>F4/80</b>	Rat	BioLegend	123110	IgG	BV421	1:100
<b>I-A/I-E</b>	Rat	BioLegend	107643	IgG	BV711	1:400
<b>I-A/I-E</b>	Rat	BioLegend	107620	IgG	PB	1:400
<b>LFA-1</b>	Rat	BioLegend	101114	IgG	AF647	1:100
<b>Ly6G</b>	Rat	BioLegend	127623	IgG	APC-Cy7	1:400
<b>Ly6G</b>	Rat	BioLegend	127605	IgG	FITC	1:200
<b>NK1.1</b>	Rat	Invitrogen	12-5941-82	IgG	PE	1:300